

Full paper

# Hierarchical Cu@CoFe layered double hydroxide core-shell nanoarchitectures as bifunctional electrocatalysts for efficient overall water splitting



Luo Yu<sup>a,b</sup>, Haiqing Zhou<sup>b</sup>, Jingying Sun<sup>b</sup>, Fan Qin<sup>c</sup>, Dan Luo<sup>b,d</sup>, Lixin Xie<sup>b</sup>, Fang Yu<sup>b</sup>, Jiming Bao<sup>c</sup>, Yong Li<sup>a</sup>, Ying Yu<sup>a,\*</sup>, Shuo Chen<sup>b,\*</sup>, Zhifeng Ren<sup>b,\*</sup>

<sup>a</sup> College of Physical Science and Technology, Central China Normal University, Wuhan 430079, China

<sup>b</sup> Department of Physics and TcSUH, University of Houston, Houston, TX 77204, USA

<sup>c</sup> Department of Electrical and Computer Engineering, University of Houston, Houston, TX 77204, USA

<sup>d</sup> Department of Chemical and Biomolecular Engineering, University of Houston, Houston, TX 77204, USA

## ARTICLE INFO

### Keywords:

Bifunctional  
Overall water splitting  
Hierarchical  
Core-shell  
Cu@CoFe LDH

## ABSTRACT

Efficient and low-cost bifunctional catalysts toward both hydrogen evolution reaction (HER) and oxygen evolution reaction (OER) for overall water splitting are of great significance to energy and environmental sustainability. Here, we report on a novel hierarchical Cu@CoFe layered double hydroxide (LDH) core-shell nanostructure catalyst for efficient overall water splitting in the alkaline medium. Benefiting from the smart structure, the optimized composite affords small overpotentials of 171 mV for the HER and 240 mV for the OER at a current density of 10 mA cm<sup>-2</sup>, along with Tafel slopes of 36.4 and 44.4 mV dec<sup>-1</sup> for the HER and OER, respectively. Strikingly, the overall water splitting performance is very good since it just requires a voltage of 1.681 V to gain a current density of 10 mA cm<sup>-2</sup>, which is only 60 mV larger than the benchmark of IrO<sub>2</sub> (+)/Pt (-) electrodes. Moreover, the optimized composite electrodes exhibit outstanding durability within 48 h testing, which is much better than that of the benchmark. Our rational design of the hierarchical core-shell nanoarchitectures presents a simple approach to fabricate advanced catalysts for water splitting.

## 1. Introduction

The depletion of fossil fuels and severe environmental problems are impelling us to explore clean and sustainable energy sources [1]. Electrochemical water splitting to produce clean fuel hydrogen (H<sub>2</sub>) from earth-abundant water (H<sub>2</sub>O) powered by renewable electricity is a promising route to alleviate energy and environment crisis [2–7]. The water electrolysis consists of two half reactions: oxygen evolution reaction (OER) and hydrogen evolution reaction (HER) [8,9]. At present, state-of-the-art HER electrocatalysts are Pt-based materials, and the best OER electrocatalysts are Ir- and Ru-based materials. However, the high cost and scarcity severely hamper their practical applications [10–12]. Until now, noble-metal-free catalysts exhibiting comparable HER performance to Pt in the acid media [13,14] and superior OER performance to RuO<sub>2</sub> and IrO<sub>2</sub> in the base media [2,11,15,16] have been reported. Regrettably, these HER catalysts are comparatively sluggish under alkaline conditions, and the activity of OER catalysts also takes a discount in the acid electrolytes [15,17]. Nevertheless, in consideration of convenience and cost for practical applications, the

electrocatalysts for HER and OER toward overall water splitting are expected to be conducted in the same electrolyte, especially in alkaline solution [15,18,19]. To overcome this drawback, it is highly desirable and imperative to design bifunctional catalysts out of non-noble metals that show satisfying activities toward both HER and OER in the alkaline or acid media.

As a family of two-dimensional (2-D) layered materials, layered double hydroxide (LDH)-based catalysts have been regarded as a promising candidate for water splitting and other energy storage due to their favorable activity, low cost, abundance, and ease of scale-up [20,21]. The general formula of LDHs is [M<sub>1</sub><sup>2+</sup><sub>1-x</sub>M<sub>2</sub><sup>3+</sup><sub>x</sub>(OH)<sub>2</sub>]<sup>q+</sup>(A<sup>n-</sup>)<sub>q/n</sub>·yH<sub>2</sub>O, in which M<sup>2+</sup> and M<sup>3+</sup> are metal cations, and A<sup>n-</sup> are charge-balancing anions [22–24]. LDHs possess a unique layered structure with the anions and water located in the interlayer of metal cations [21], which are favorable for diffusion of water molecules, ensuring intimate contact with the catalyst. Also, the interlayer spacing is beneficial to the release of gaseous products [25]. In 2014, Grätzel et al. reported that NiFe LDH/Ni foam exhibited high activity toward both OER and HER in alkaline electrolyte, and the combination of the two yielded a current

\* Corresponding authors.

E-mail addresses: [yuying01@mail.ccnu.edu.cn](mailto:yuying01@mail.ccnu.edu.cn) (Y. Yu), [schen34@uh.edu](mailto:schen34@uh.edu) (S. Chen), [zren@uh.edu](mailto:zren@uh.edu) (Z. Ren).

density of  $10 \text{ mA cm}^{-2}$  under a voltage of  $\sim 1.7 \text{ V}$  [5]. Subsequently, diverse kinds of LDHs with various morphologies including CoFe LDH nanosheets [24] and exfoliated NiFe LDH single-layer nanosheets [26] with superior OER performances as well as LDHs-based composites like CoSe/NiFe LDH/graphene [15] and NiFe LDH/NiCo<sub>2</sub>O<sub>4</sub> [27] with decent activity for overall water splitting have been further studied.

One-dimensional (1-D) hierarchical core-shell nanostructures are extremely attractive owing to their large surface area with plenty of active sites and efficient electron transport within the smallest dimensions [28,29]. As the core, it is preferable to own an excellent conductivity for efficient electron transport. Lately, Qu and coworkers designed MoSe<sub>2</sub>/Mo core-shell hierarchical nanostructures as efficient HER catalysts for water splitting [30]. Provoked by the aforesaid contents, herein, we combine 1-D Cu nanowires (NWs) and 2-D CoFe LDH nanosheets (NSs) to fabricate a novel hierarchical core-shell nanoarchitecture on Cu foams for efficient water splitting. Benefiting from the smart structure, the hierarchical core-shell nanoarchitectures exhibit highly improved activity and outstanding stability toward both HER and OER in alkaline medium, thus functioning as a versatile electrode for efficient overall water splitting.

## 2. Experimental section

### 2.1. Chemicals

Hydrochloric acid (HCl, AR, MACRON), ethanol (C<sub>2</sub>H<sub>5</sub>OH, Decon Labs, Inc.), sodium hydroxide (NaOH, AR, MACRON), ammonium persulfate [(NH<sub>4</sub>)<sub>2</sub>S<sub>2</sub>O<sub>8</sub>, 98%, Sigma-Aldrich], potassium bicarbonate (KHCO<sub>3</sub>, 99.7%, Sigma-Aldrich), cobalt(II) nitrate hexahydrate (Co(NO<sub>3</sub>)<sub>2</sub>·6H<sub>2</sub>O, 98%, Sigma-Aldrich), iron(II) sulfate heptahydrate (FeSO<sub>4</sub>·7H<sub>2</sub>O,  $\geq 99.95\%$ , Sigma-Aldrich), nafion 117 solution (5%, Sigma-Aldrich), iridium oxide powder (IrO<sub>2</sub>, 99%, Alfa Aesar), potassium hydroxide (KOH, 50% w/v, Alfa Aesar), and Cu foam (thickness: 1.5 mm) were used as received. Deionized water (18.3 M $\Omega$  cm resistivity) was used for the preparation of all aqueous solutions.

### 2.2. Fabrication of Cu@CoFe LDH on Cu foam

Firstly, Cu(OH)<sub>2</sub> nanorods (NRs) were synthesized through a chemical oxidation method, and a typical process was as follows. A piece of Cu foam with a size of  $2 \times 5 \text{ cm}^2$  was cleaned in hydrochloric acid (37%) and then cleaned ultrasonically in ethanol and deionized water for 15 min sequentially. The cleaned Cu foam was then immersed into 80 mL of an aqueous solution containing 2.5 M NaOH and 0.125 M (NH<sub>4</sub>)<sub>2</sub>S<sub>2</sub>O<sub>8</sub> for 20 min. Finally, the Cu foam with a light blue color was taken out from the solution, rinsed with deionized water, and dried in air. Afterward, the prepared Cu(OH)<sub>2</sub> NRs were calcined at 180 °C in the air for 1 h to obtain CuO nanowires (NWs). The electrochemical reduction of CuO to Cu was conducted in Ar purged KHCO<sub>3</sub> solution at  $-0.4 \text{ V}$  (vs. reversible hydrogen electrode, RHE). When the cathodic current reached to steady and near-zero, the reduction was complete. The electrodeposition of CoFe LDH was carried out in a three-electrode configuration, by using as-prepared Cu NWs/Cu foam, Pt net and saturated calomel electrode (SCE) as the working, counter and reference electrode, respectively. The electrolyte was obtained by dissolving Co(NO<sub>3</sub>)<sub>2</sub>·6H<sub>2</sub>O (0.15 M) and FeSO<sub>4</sub>·7H<sub>2</sub>O (0.15 M) in 100 mL water with a continuous Ar flow to prevent the oxidation of Fe<sup>2+</sup>. The applied potential was  $-1.0 \text{ V}$  vs. SCE, and different electrodeposition time with 30, 60, 90, and 120 s were used to control the thickness and morphology of the composites. The samples were successively labeled with CCF LDH-30, CCF LDH-60, CCF LDH-90, and CCF LDH-120, respectively. For comparison, pure CoFe LDH was synthesized on Cu foam by the same method for 60 s, which was labeled with CF LDH.

### 2.3. Preparation of IrO<sub>2</sub> electrode on Cu foam

To prepare the IrO<sub>2</sub> electrode, 40 mg IrO<sub>2</sub> and 60  $\mu\text{L}$  Nafion, 540  $\mu\text{L}$  ethanol and 400  $\mu\text{L}$  deionized water were ultrasonicated for 30 min to obtain a homogeneous dispersion. Then, the dispersion was coated onto a cleaned Cu foam, which was then dried in air overnight at room temperature. The loading of IrO<sub>2</sub> catalyst on Cu foam is  $\sim 1.8 \text{ mg cm}^{-2}$ , just the same with that of CCF LDH-60.

### 2.4. Materials characterization

The morphology and crystal structure of the samples were detected with scanning electron microscopy (SEM, LEO 1525) and transmission electron microscope (TEM, JEOL 2010F) coupled with energy dispersive X-ray (EDX) spectroscopy. The phase composition of the samples was characterized by X-ray diffraction (PANalytical X'pert PRO diffractometer with a Cu K $\alpha$  radiation source). X-ray photoelectron spectroscopy (XPS) (PHI Quantera XPS) was performed using a PHI Quantera SXM Scanning X-ray Microprobe.

### 2.5. Electrochemical tests

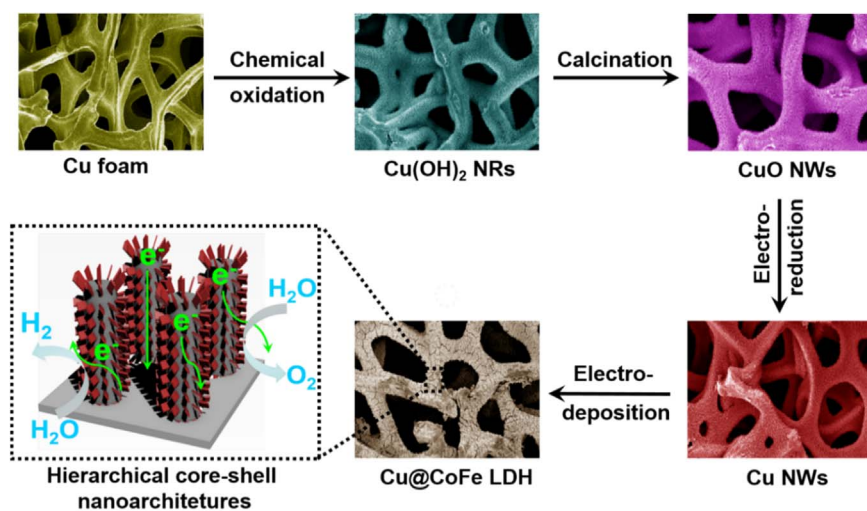
Electrochemical measurements were carried out on an electrochemical station (SP-150) in a standard three-electrode system with the prepared samples as the working electrode, a Pt net as the counter electrode, and a standard Hg/HgO electrode as the reference. The OER activity was evaluated using linear sweep voltammetry (LSV) with a sweep rate of  $2 \text{ mV s}^{-1}$  and chronopotentiometry at a constant current density of  $10 \text{ mA cm}^{-2}$  in O<sub>2</sub>-saturated 1 M KOH solution. The HER tests were performed in Ar-saturated 1 M KOH solution. Cyclic voltammetry (CV) curves were collected at different scan rates in the potentials from 1.025V to 1.125 V vs RHE to evaluate the double-layer capacitance values. Electrochemical impedance spectroscopy (EIS) was measured at an overpotential of 250 mV from 0.1 Hz to 100 kHz with an amplitude of 10 mV. The overall water splitting performance was evaluated in 1 M KOH using a two-electrode configuration, and the polarization curve was recorded at a scan rate of  $2 \text{ mV s}^{-1}$ . All the measured potentials vs. the Hg/HgO were converted to RHE by the Nernst equation ( $E_{\text{RHE}} = E_{\text{Hg/HgO}} + 0.0591\text{pH} + 0.098$ ). All the curves were reported with iR compensation.

## 3. Results and discussion

Scheme 1 shows the preparation process of Cu@CoFe LDH core-shell nanoarchitectures. Briefly, Cu(OH)<sub>2</sub> nanorods (NRs) were synthesized through chemical oxidation of a Cu foam, which was followed by calcination to form CuO NWs. Cu NWs was obtained by electroreduction of CuO. The CoFe LDH nanosheets were then electrodeposited on the Cu NWs to finally form the Cu@CoFe LDH core-shell nanoarchitectures. Fig. S1 presents the optical pictures of as-prepared samples, showing

the apparent color change and equalmente growth of active materials. Fig. S2 displays the SEM images of the starting Cu foam, exhibiting a three-dimensional (3-D) porous structure, which is a good candidate for 3-D skeletons. The SEM images of Cu(OH)<sub>2</sub> NRs, CuO NWs, and Cu NWs with different magnifications are presented in Fig. S3, all of which showed dense 1-D structure and were closely attached to the 3-D support. Pure CoFe LDH (labeled with CF LDH) was also synthesized on the Cu foam for comparison, and the SEM images are displayed in Fig. S4, which showed many nanosheets compactly grew on the surface of the Cu foam.

Fig. 1a are the SEM and TEM images (inset) of Cu NWs, which preserved the 1-D structure of CuO NWs with slightly curved due to the electroreduction force. The diameter and length of Cu NWs were  $\sim 200 \text{ nm}$  and  $\sim 2.5 \mu\text{m}$ , respectively. After 1 min electrodeposition of CoFe LDH (the composite is named by CCF LDH-60), the Cu NWs



Scheme 1. Fabrication process of Cu@CoFe LDH core-shell nanostructure electrocatalysts.

surface became thicker, and many nanosheet branches uniformly decorated the nanowire surface, as shown in Fig. 1b. The TEM image (inset of Fig. 1b) clearly shows that the nanosheets were interconnected with each other, forming a highly porous surface morphology. The transparent character of the nanosheet shell indicated their extremely thin thickness. Fig. 1c displays a typical TEM image of an individual hybrid nanostructure, which distinctly exhibited the core-shell

structure of the composite. The diameter of the core-shell hybrid was  $\sim 1 \mu\text{m}$  with  $\sim 200 \text{ nm}$  core of Cu NWs and  $\sim 400 \text{ nm}$  shell of CoFe LDH NSs. SEM images of the composites with different electrodeposition time (30, 60, 90, and 120 s) of CoFe LDH are presented in Fig. S5 to study the morphology variation. The samples are successively labeled with CCF LDH-30, CCF LDH-60, CCF LDH-90, and CCF LDH-120. It can be observed that the thickness of the hybrid quickly increased when the

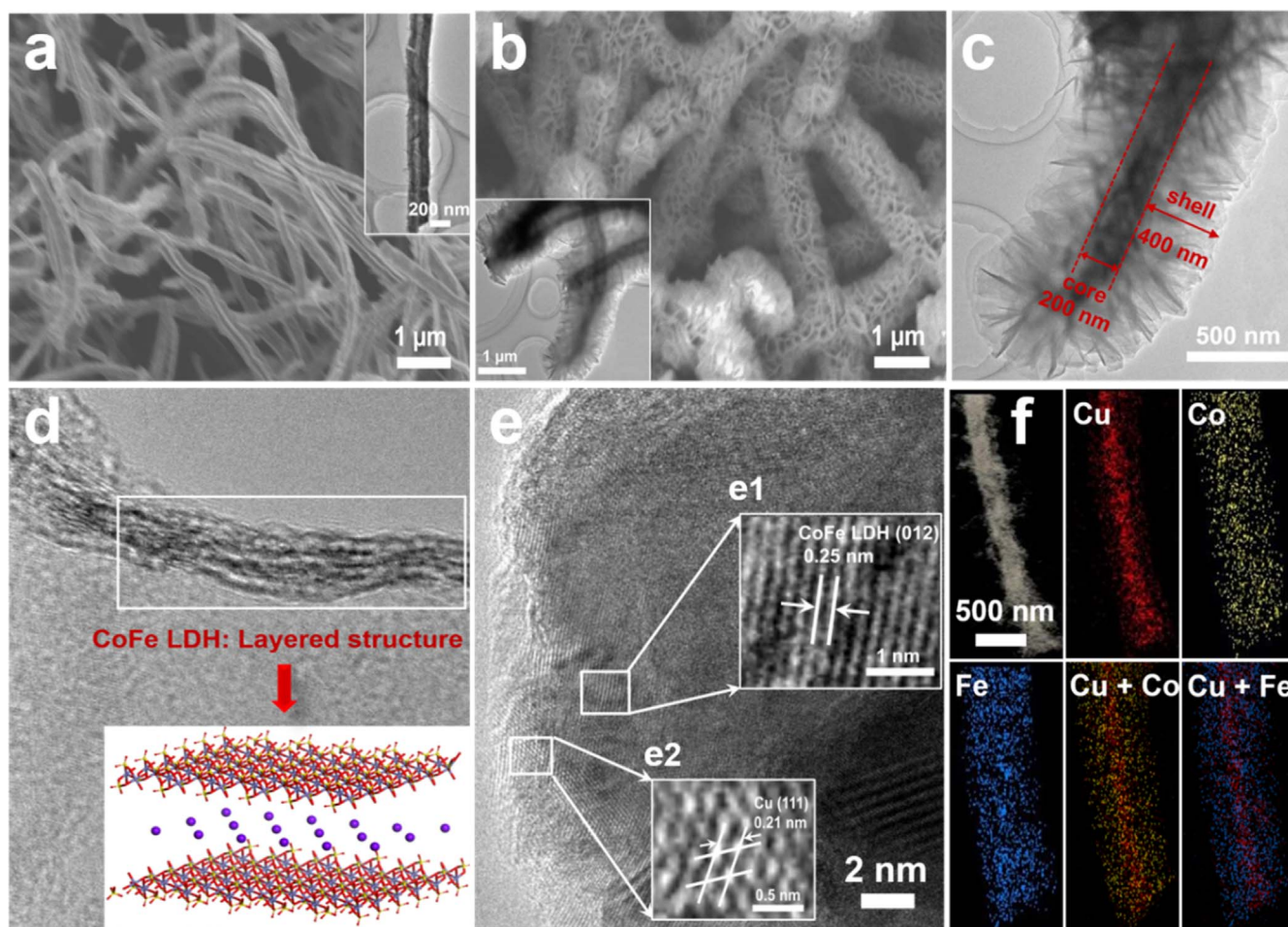


Fig. 1. SEM images of (a) Cu NWs and (b) CCF LDH-60. (The insets are the corresponding TEM images.) (c) TEM image of CCF LDH-60 at medium magnification. HRTEM image of CCF LDH-60 to show (d) the layered structure of CoFe LDH and (e) its lattice fringes. (The inset in d is a structure model of CoFe LDH. (e1) and (e2) in e are the corresponding enlarged parts of the square.) (f) DF-STEM image of CCF LDH-60 and the corresponding elemental mapping.

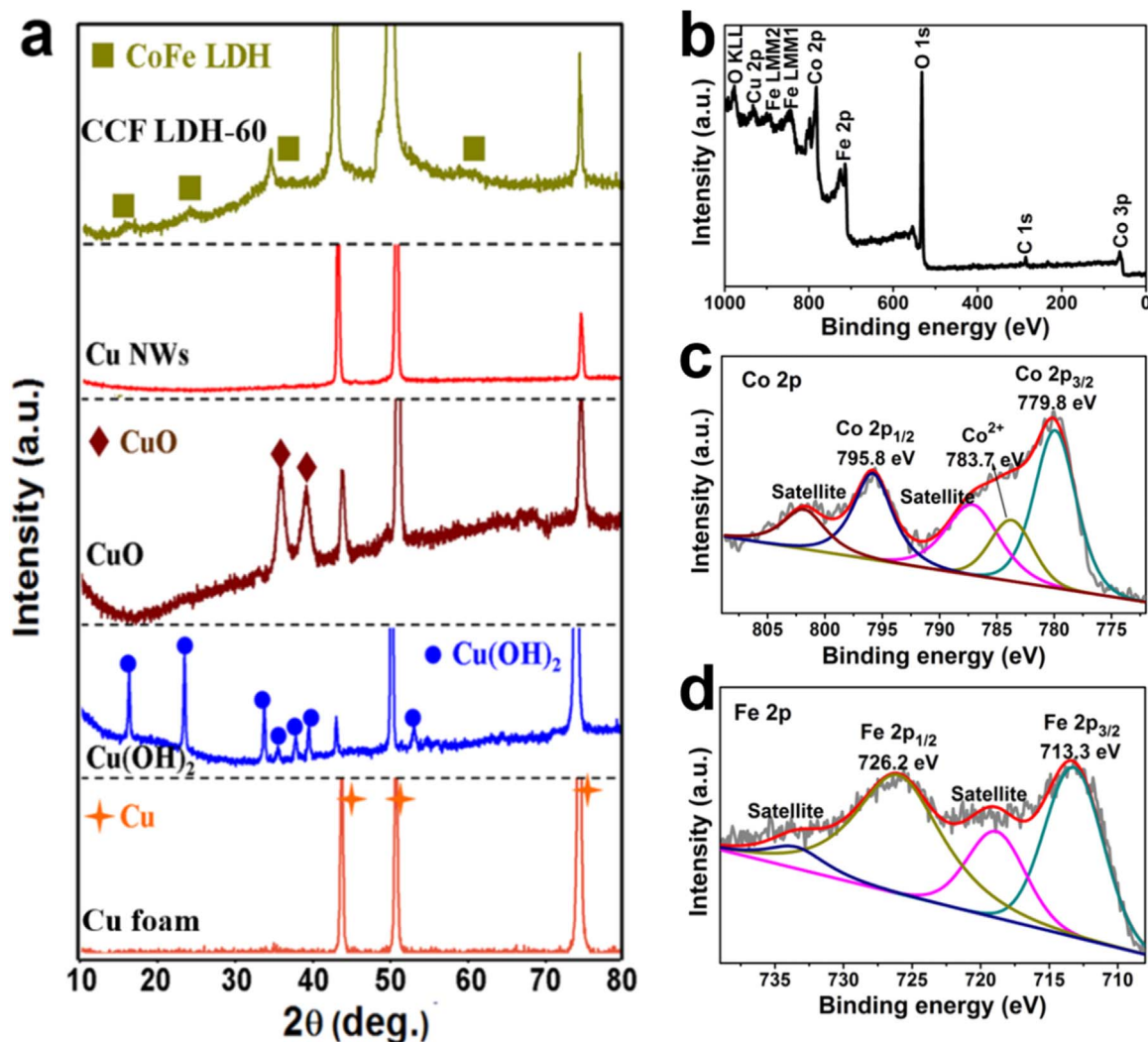


Fig. 2. (a) XRD patterns of as-prepared samples. (b) XPS spectrum of CCF LDH-60. High-resolution XPS spectra of (c) Co 2p and (d) Fe 2p for CCF LDH-60, located at 713.3 and 726.2 eV corresponded to Fe 2p<sub>3/2</sub> and Fe 2p<sub>1/2</sub>, respectively [36]. And two satellite peaks were located at 718.9 and 733.8 eV, indicating the Fe<sup>3+</sup> oxidation state.

electrodeposition time was prolonged, and CCF LDH-120 was mostly agglomerated. The high-resolution TEM (HRTEM) image of CCF LDH-60 in Fig. 1d clearly shows the layered structure of out-shell of CoFe LDH, and the inset of Fig. 1d presents the structural model of CoFe LDH. The layered structure allows the fast electron transport and avails the diffusion of H<sub>2</sub>O molecules, ensuring intimate contact between the catalyst and electrolyte during electrolysis [25]. The HRTEM image in Fig. 1e reveals the interplanar spacing of  $\sim 0.25$  nm for CoFe LDH (inset as e1) and  $\sim 0.21$  nm for Cu (inset as e2), corresponding to the (012) plane of LDH and (111) plane of Cu, respectively, which are consistent with literature results [24,31]. Dark-field scanning transmission electron microscopy (DF-STEM) and the corresponding elemental mapping of a single hybrid nanowire, shown in Fig. 1f, unambiguously confirm the Cu NWs@CoFe LDH NSs core-shell structure and uniform distribution of Cu, Co, and Fe elements in the composites. EDX spectra in Fig. S6 further determined the atomic ratio of Cu, Co, and Fe for the three composites, and the atomic ratio of Co to Fe in the CCF LDH-60 is around 1.57:1.

Fig. 2a shows the XRD patterns of Cu foam substrate, Cu(OH)<sub>2</sub> NRs, CuO NWs, Cu NWs and CCF LDH-60, which are identified as pure phase with high crystallinity. After electroreduction, the peaks of CuO disappeared with three peaks from Cu retaining, indicating totally transformation from CuO to Cu. After decorated with the CoFe LDH, four new peaks emerged on the XRD pattern of CCF LDH-60, which were

assigned to CoFe LDH [32]. The elemental composition and chemical state in the composites were further studied by the X-ray photoelectron spectroscopy (XPS). As depicted in Fig. 2b, the full XPS spectrum of CCF LDH-60 revealed the signals of Cu, Co, Fe, O and C (for calibration) elements, which was consistent with the EDX results in Fig. S6. Fig. 2c and d are the high-resolution XPS spectra of Co 2p and Fe 2p, respectively. As shown in Fig. 2c, the two peaks located at binding energy of 779.8 and 795.8 eV were assigned to Co 2p<sub>3/2</sub> and Co 2p<sub>1/2</sub>, respectively, along with two satellite peaks at 787.2 and 801.7 eV [33,34]. The spin-orbit splitting value of 2p<sub>1/2</sub> and 2p<sub>3/2</sub> reaches  $\sim 16$  eV, suggesting that the Co oxidation state was mainly Co<sup>2+</sup> [35]. The peak at binding energy of 783.7 eV was also attributed to Co<sup>2+</sup> [19]. For the XPS spectra of Fe 2p (Fig. 2d), two prominent peaks

The OER and HER activities of the as-prepared electrodes were evaluated in 1 M KOH aqueous electrolyte using a standard three-electrode system. All potentials were iR-corrected and converted to a reversible hydrogen electrode (RHE) scale. Fig. 3a shows

the polarization curves of as-prepared electrodes at a scan rate of 2 mV s<sup>-1</sup>. As expected, the Cu@CoFe LDH core-shell nanoarchitectures displayed much lower overpotentials at the same current density compared with pure CoFe LDH, Cu NWs, and bare Cu foam. Glaringly, CCF LDH-60 even outperformed the IrO<sub>2</sub>/Cu foam electrode, revealing the highest OER activity among the three composites. To give a detailed comparison, the overpotentials at the current densities of 10 and

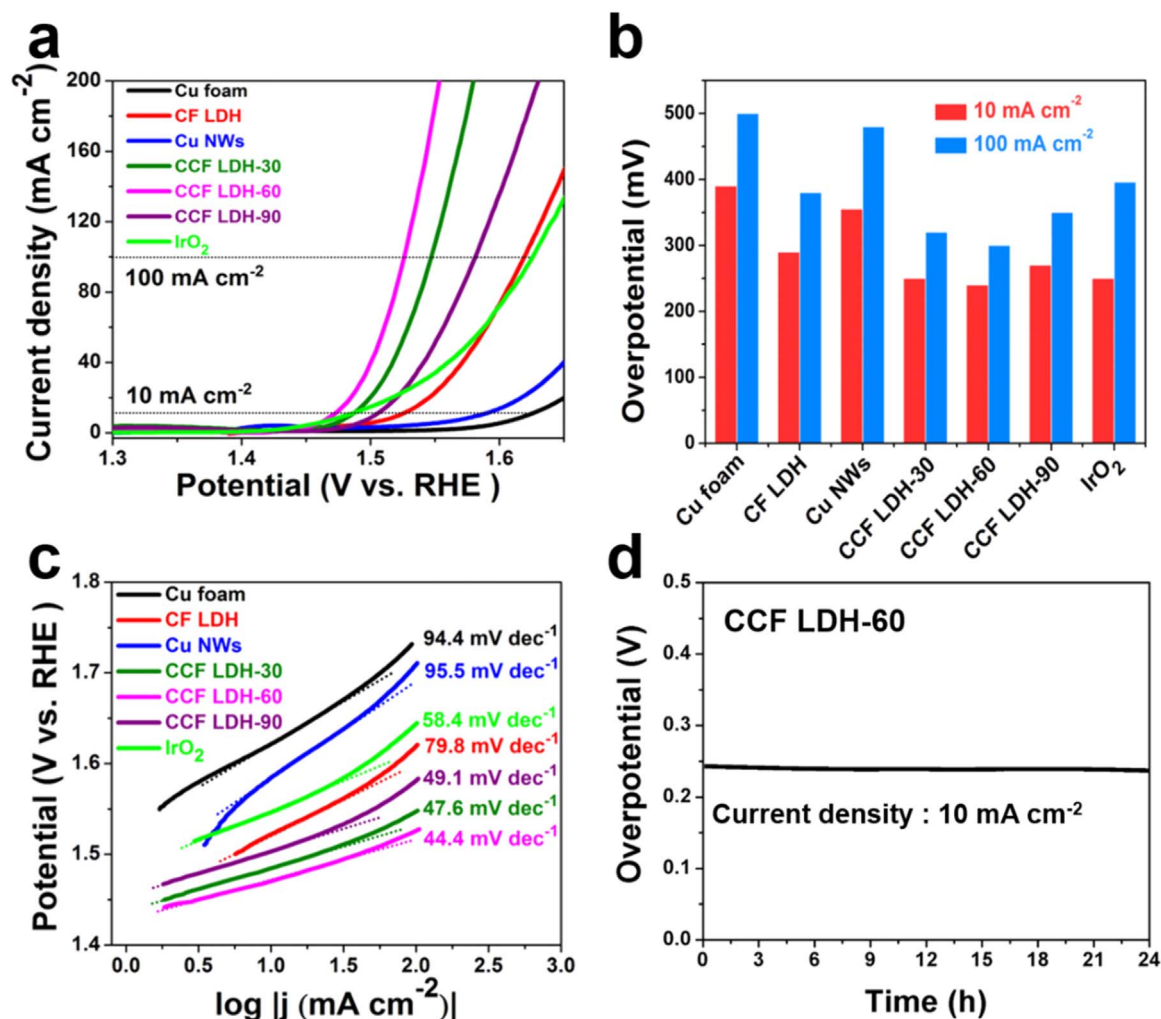


Fig. 3. (a) Polarization curves, (b) overpotentials (at 10 and 100 mA cm<sup>-2</sup>) and (c) Tafel plots of as-prepared samples. (d) Chronopotentiometry curves of CCF LDH-60 at a constant current density of 10 mA cm<sup>-2</sup>. All the tests were conducted in 1 M KOH electrolyte.

100 mA cm<sup>-2</sup> for the various electrodes are presented in Fig. 3b. To achieve a current density of 10 mA cm<sup>-2</sup>, CCF LDH-60 required an overpotential of 240 mV, which was 50, 105, 10, 30, and 10 mV less than those of CF LDH, Cu NWs, CCF LDH-30, CCF LDH-90, and commercial IrO<sub>2</sub>/Cu foam, respectively. Similarly, the overpotential of CCF LDH-60 at a high current density of 100 mA cm<sup>-2</sup> was 300 mV, which was also the lowest among all the catalysts. The detailed data for the electrodes are summarized in Table S1. Moreover, as shown in Fig. S7a, this performance was better than those of Cu@Co(OH)<sub>2</sub> and Cu@FeOOH, suggesting a synergistic effect between Co and Fe in the composite for the improved OER activity. We further evaluated the mass activity of our catalysts normalized by the mass of CoFe LDH (Fig. S8a), and we can see that the OER mass activity of the core-shell Cu@CoFe LDH catalysts was better than that of pure CoFe LDH (CF LDH). The best sample of CCF LDH-60 can deliver current densities of 10 and 100 mA mg<sup>-1</sup> at overpotentials of 252 and 318 mV, respectively. Fig. 3c shows the corresponding Tafel plots of the electrodes. The Tafel slope of CCF LDH-60 was 44.4 mV dec<sup>-1</sup>, which was smaller than all the other electrodes including IrO<sub>2</sub>/Cu foam, indicating the favorable catalytic kinetics. Long time stability test of CCF LDH-60 was also conducted at a constant current density of 10 mA cm<sup>-2</sup>. As displayed in Fig. 3d, the overpotential to achieve a current density of 10 mA cm<sup>-2</sup> was stable at ~240 mV for 24 h, confirming the remarkable durability. Table S2 gives a detailed comparison of the OER performance for CCF LDH-60 catalyst with other reported catalysts in 1 M alkaline electrolytes, from which we can see that the Cu@CoFe LDH core-shell

nanoarchitectures outperform most of LDH-, Co-, and Fe-based catalysts.

The catalytic ability of the core-shell catalysts for HER was also assessed in 1 M KOH solution to inspect the possibility for overall water splitting. As the polarization curves shown in Fig. 4a, the Cu@CoFe LDH exhibited much higher HER activity than those of CoFe LDH, Cu NWs, and bare Cu foam. Notably, the commercial Pt wire was still the best with negligible overpotentials. Fig. 3b shows the overpotentials at current densities of -10 and -100 mA cm<sup>-2</sup> for the electrodes to give a detailed comparison. CCF LDH-60 required an overpotentials of 171 and 197 mV to obtain current densities of -10 and -100 mA cm<sup>-2</sup>, respectively, which were much smaller than those of CF LDH, Cu NWs, CCF LDH-30 and CCF LDH-90. The differences with commercial Pt wire were 88 and 89 mV for -10 and -100 mA cm<sup>-2</sup>, respectively. Similarly, the HER activity of CCF LDH-60 was also much better than those of Cu@Co(OH)<sub>2</sub> and Cu@FeOOH (Fig. S7b), suggesting a synergistic effect between Co and Fe in the composite sample for the enhanced HER activity. The mass activity normalized by the mass of CoFe LDH in Fig. S8b showed that the CCF LDH-60 sample can deliver current densities of 10 and 100 mA mg<sup>-1</sup> at overpotentials of 177 and 204 mV, respectively, which was much better than the CCF LDH-30, CCF LDH-90, and CF LDH. Impressively, the Tafel slope (Fig. 4c) of CCF LDH-60 was 36.4 mV dec<sup>-1</sup>, which was very close to the commercial Pt wire and smaller than the other electrodes. Additionally, the HER stability test of CCF LDH-60 conducted at a constant overpotential of 178 mV is displayed in Fig. 3d, from which we can observe that the current

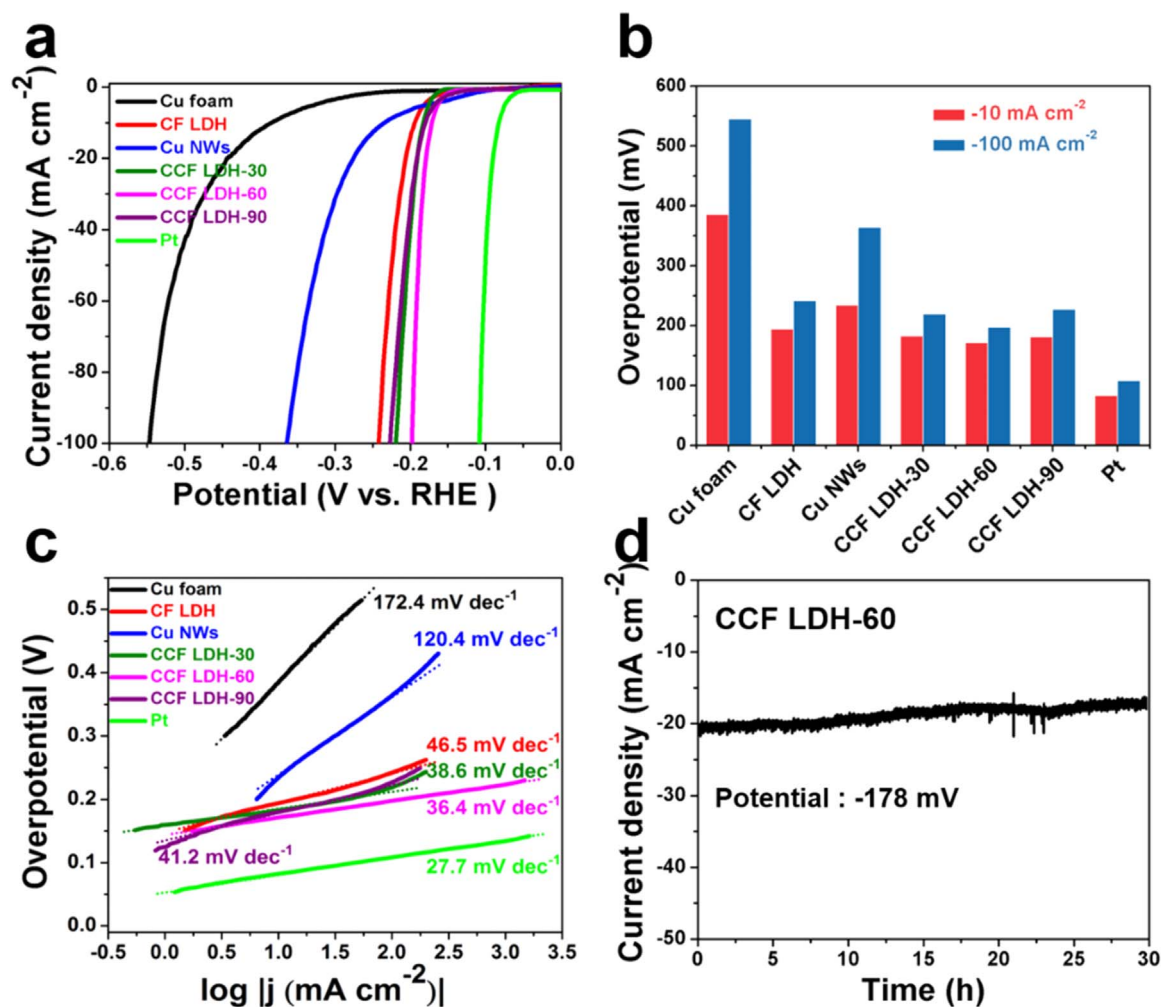


Fig. 4. (a) Polarization curves, (b) overpotentials (at  $-10$  and  $-100$   $\text{mA cm}^{-2}$ ) and (c) Tafel plots of as-prepared samples. (d) Time dependence of the current density for CCF LDH-60 under a constant overpotential of  $178$  mV to afford a current density of  $20$   $\text{mA cm}^{-2}$ . All the tests were conducted in  $1$  M KOH electrolyte.

density was almost stable with little decay during  $30$  h testing. Therefore, our Cu@CoFe LDH core-shell catalysts are also decent catalysts for HER in the strong base electrolyte. The detailed comparison of the HER performance for CCF LDH-60 with other reported catalysts in  $1$  M alkaline electrolytes is listed in Table S3. Although the HER performance of CCF LDH-60 is inferior to that of commercial Pt, it is still competitive with those of non-noble metal-based catalysts.

The above results verify that our rational design of the hierarchical Cu@CoFe LDH core-shell nanoarchitectures are efficient bifunctional catalysts toward both HER and OER in the alkaline media. Subsequently, we evaluated the overall water splitting performance in a home-made electrolyser with a two-electrode system by using the CCF LDH-60 electrode as both anode and cathode. As shown in Fig. 5a, CCF LDH-60 electrodes delivered a current density of  $10$   $\text{mA cm}^{-2}$  at an operating voltage of  $1.681$  V, which is only  $60$  mV larger than the benchmark of  $\text{IrO}_2$  (+)/Pt (-) electrodes. Obvious  $\text{H}_2$  and  $\text{O}_2$  bubbles (inset in Fig. 5a) were observed on the surface of both electrodes during linear sweep voltammetry (LSV) tests. This performance is superior to many Co- and Ni-based bifunctional catalysts and comparable to some robust materials for overall water splitting (Table S4). The long-term stability test was further conducted by full water splitting at a constant current density of  $10$   $\text{mA cm}^{-2}$  in a two-electrode configuration. The benchmark electrodes of  $\text{IrO}_2$  (+)/Pt (-) exhibited a gradual increase of overpotential in  $24$  h, indicating their instability. In contrast, the overpotential of CCF LDH-60 electrodes was almost stable for over  $48$  h continuous testing (Fig. 5b). Finally, the gaseous products from the

overall water splitting by the CCF LDH-60 electrodes were determined using

gas chromatography. As shown in Fig. 5c, only  $\text{H}_2$  and  $\text{O}_2$  with a predicted ratio of  $2:1$  were detected, and the amount of measured  $\text{H}_2$  and  $\text{O}_2$  matched well with those calculated results, indicating the nearly  $100\%$  Faradaic efficiency.

It is generally acknowledged that the electrochemical water splitting process mainly involves three steps. The first is the adsorption of water molecules onto the electrode surface, second the water reduction (HER) and oxidation (OER) on the active sites, and third the gas products releasing [25]. Our rational design of the hierarchical core-shell nanoarchitectures is expected to offer a large surface area, and the layered structure of CoFe LDH further increases the accessible surface area and exposes more active sites, all of which are beneficial to the first step of water molecules adsorption. The effective surface area can be determined by measuring the electrochemical double-layer capacitance ( $C_{dl}$ ) through cyclic voltammetry (CV) tests at different scan rates [37]. Fig. 5d shows the capacitive currents as a function of scan rate obtained from corresponding CV curves (inset in Fig. 5d and Fig. S9) to calculate  $C_{dl}$  for the electrodes. We can see that the  $C_{dl}$  values of the core-shell nanoarchitectures were much larger than those of bare Cu NWs and CoFe LDH on Cu foams, demonstrating the improved surface area and active sites achieved by the rational design of the hierarchical core-shell structure. The  $C_{dl}$  value was determined to be  $75.3$   $\text{mF cm}^{-2}$  for CCF LDH-60, which was larger than the  $65.1$   $\text{mF cm}^{-2}$  for CCF LDH-30 and  $31.8$   $\text{mF cm}^{-2}$  for CCF LDH-90. This is mainly because excessive CoFe

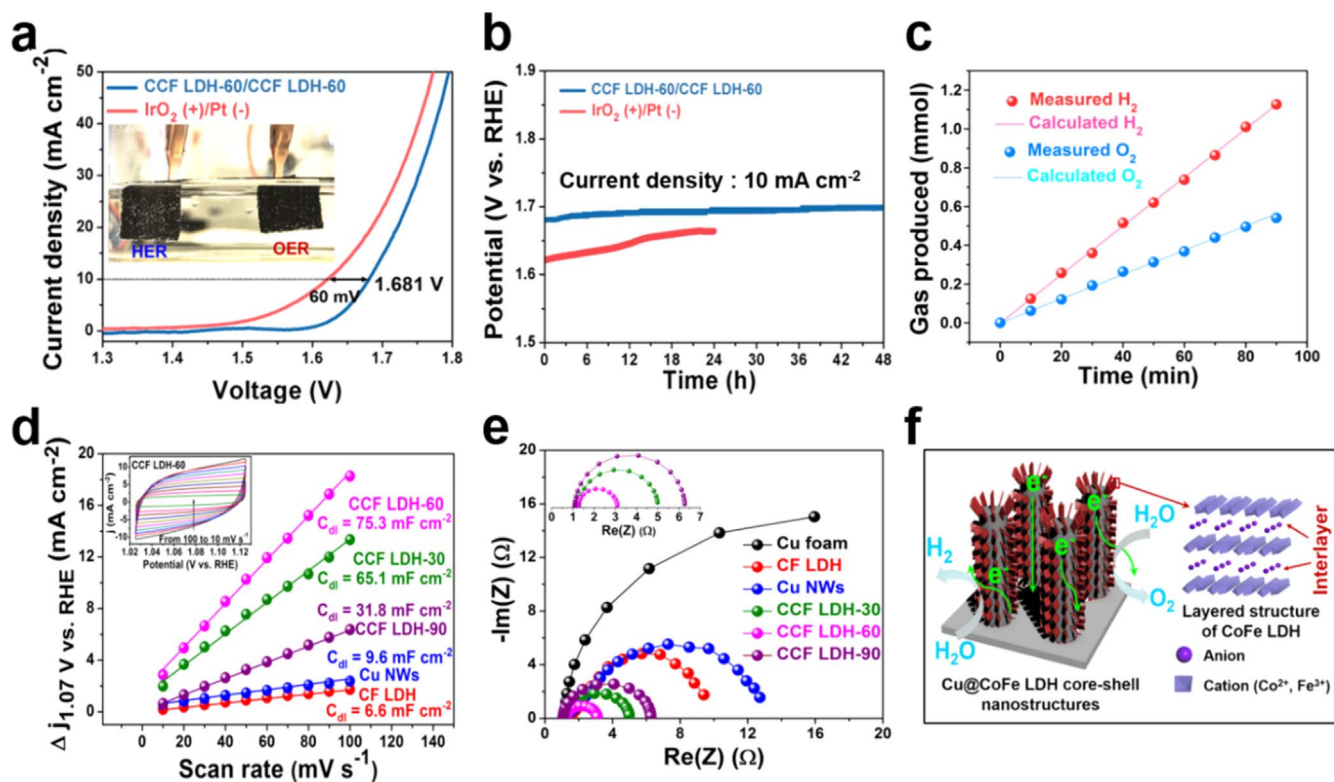


Fig. 5. (a) Polarization curves for overall water splitting with the CCF LDH-60 electrode as both anode and cathode at a scan rate of  $2 \text{ mV s}^{-1}$ . (The inset is the optical photograph showing the generation of  $\text{H}_2$  and  $\text{O}_2$  bubbles on the electrodes.) (b) Chronopotentiometry curves of CCF LDH-60 at a constant current density of  $10 \text{ mA cm}^{-2}$  in a two-electrode configuration. The benchmark electrodes of  $\text{IrO}_2 (+)/\text{Pt} (-)$  are tested side by side shown in a and b. (c) Experimental and theoretical amounts of  $\text{H}_2$  and  $\text{O}_2$  by the CCF LDH-60 electrode at a fixed current density of  $40 \text{ mA cm}^{-2}$ . (d) Capacitive currents as a function of scan rate and (e) the enlarged EIS curves of the composites. All the tests were conducted in  $1 \text{ M KOH}$  electrolyte. (f) Schematic illustration of structure characteristics for the hierarchical  $\text{Cu@CoFe LDH}$  core-shell nanostructure electrode.

LDH nanosheets attached on the Cu NWs may block the interconnection between the nanosheets, and some agglomerations even formed for the CCF LDH-90 as shown in the Fig. S5c. For the second step of water reduction and oxidation on the active sites, the hierarchical core-shell nanoarchitectures offer more accessibility of active sites. Moreover, the superior electrical conductivity enables fast electron transport in Cu nanowires, which facilitates the reaction kinetics [19,38]. This viewpoint is authenticated by the electrochemical impedance spectroscopy (EIS). As the Nyquist plots shown in Fig. 5e, the charge-transfer resistance ( $R_{ct}$ ) for the core-shell composites was much smaller than those of pure CoFe LDH, Cu NWs, and Cu foam alone, revealing more desirable electron transport and catalytic kinetics. The fitted data of the samples are listed in Table S1. Meanwhile, all the catalysts exhibited very small series resistances ( $R_s$ ,  $\sim 1 \Omega$ ), indicating the high-quality electrical integration of the catalysts and Cu foam [1,6,39]. Of note, no polymer binder or conductive additives were used to prepare electrodes, which substantially reduces the electrode dead volume [25,40]. As for the last step of gas products releasing, the hierarchical core-shell nanoarchitectures provide large open space for the release of gas bubbles, enhancing the contact between electrolyte and active sites [19,41,42]. Meanwhile, the interlayer spacing of CoFe LDH is also propitious to gaseous products releasing. Based on the discussion, a schematic illustration of structure characteristics for the hierarchical  $\text{Cu@CoFe LDH}$  core-shell nanoarchitectures is presented in Fig. 5f.

The catalyst loading of CoFe LDH for CCF LDH-90 ( $2.4 \text{ mg cm}^{-2}$ ) was more than those of CCF LDH-30 ( $1.3 \text{ mg cm}^{-2}$ ) and CCF LDH-60 ( $1.8 \text{ mg cm}^{-2}$ ), but the HER and OER performance of CCF LDH-90 was inferior to the other two, indicating that the quintessential core-shell nanostructure plays a vital role for the catalytic reactions. Therefore, we took SEM and TEM images of CCF LDH-60 after overall water splitting stability test for 48 h to probe the possible structure changes.

As shown in Fig. 6a, on the anode side for OER, the SEM and TEM images revealed that the core-shell architecture of CCF LDH-60 was well preserved, and the diameter of the hybrid became a little smaller with some loss of branching nanosheets. Meanwhile, the (012) plane of CoFe

LDH with the interplanar spacing of  $0.25 \text{ nm}$  is still detectable from the HRTEM image in Fig. 6c, the EDS mapping images further confirm the intact core-shell nanostructure and homogeneous distribution of the elements. The same situation is also observed on the cathode side for HER in Fig. S10. We further conducted XPS for CCF LDH-60 after overall water splitting stability test to examine the composition change of Co and Fe on the surface. As shown in Fig. S11, the full spectra along with the high-resolution XPS spectra of Co 2p and Fe 2p of CCF LDH-60 for the anode (OER) and cathode (HER) after stability test are almost the same with that of the fresh sample, meaning no composition change of Co and Fe. A slight change is that the peak intensity decreased after stability test, which was probably due to the small loss of CoFe LDH nanosheets. However, this does not decay the activity for water splitting. As shown in Fig. S12, compared with the initial, the  $R_{ct}$  of CCF LDH-60 after stability test just increased  $0.65$  and  $0.6 \Omega$  for OER and HER, respectively. More importantly, the activity of OER and HER for CCF LDH-60 was almost maintained (Fig. 6d). Therefore, our rational design of this hierarchical  $\text{Cu@CoFe LDH}$  core-shell nanoarchitectures are efficient and robust bifunctional catalysts toward overall water splitting.

#### 4. Conclusions

In summary, a smart hierarchical  $\text{Cu@CoFe LDH}$  core-shell nanostructure composite was fabricated as an efficient and low-cost bifunctional catalyst for overall water splitting. The rational design of this

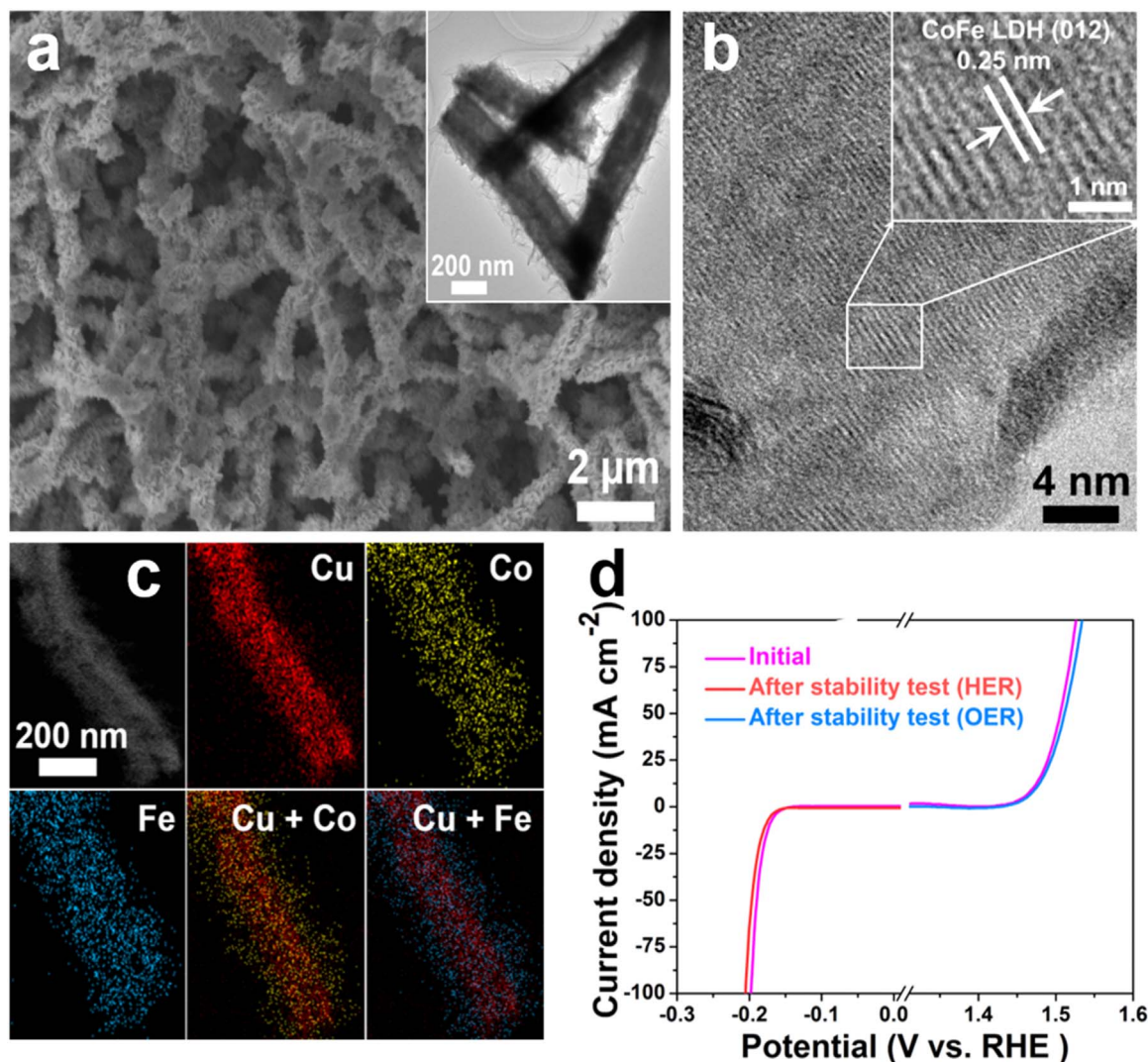


Fig. 6. (a) SEM and TEM (inset) images, (b) HRTEM image, and (c) EDS elemental mapping images of CCF LDH-60 after overall water splitting stability test (anode for OER). (d) Polarization curves of CCF LDH-60 before and after overall water splitting stability test.

hierarchical core-shell nanostructure endows the composite with a large surface area and accessibility of active sites, which are beneficial for the adsorption of water molecules and catalytic reactions. Moreover, the unique layered structure of CoFe-LDH NSs are favorable for diffusion of water molecules and release of gas products, ensuring intimate contact between the catalyst and electroactive species. In addition, the Cu NWs cores provide highways for electron transport, decreasing the electron transport distance and barrier, which facilitates the reaction kinetics. Benefitting from these advantages, the Cu@CoFe LDH core-shell catalysts exhibit excellent performance for overall water splitting in the alkaline medium. Above all, our rational design of hierarchical core-shell nanoarchitectures presents a facile approach to fabricate advanced materials for energy and environmental fields.

#### Acknowledgements

The work is partially supported by the China Scholarship Council, National Natural Science Foundation of China (Nos. 21377044 and 21573085), and the work performed at the University of Houston is funded by the US Department of Energy under Award number DE-SC0010831.

#### Appendix A. Supporting information

Supplementary data associated with this article can be found in the online version at <http://dx.doi.org/10.1016/j.nanoen.2017.09.045>.

#### References

- [1] H. Zhou, F. Yu, Y. Huang, J. Sun, Z. Zhu, R.J. Nielsen, R. He, J. Bao, W.A. Goddard III, S. Chen, Z. Ren, *Nat. Commun.* 7 (2016) 12765–12771.
- [2] Y. Hou, M.R. Lohe, J. Zhang, S. Liu, X. Zhuang, X. Feng, *Energy Environ. Sci.* 9 (2016) 478–483.
- [3] Y. Jiao, Y. Zheng, M. Jaroniec, S.Z. Qiao, *Chem. Soc. Rev.* 44 (2015) 2060–2086.
- [4] Y.P. Zhu, C. Guo, Y. Zheng, S.Z. Qiao, *Acc. Chem. Res.* 50 (2017) 915–923.
- [5] J. Luo, J.H. Im, M.T. Mayer, M. Schreier, M.K. Nazeeruddin, N.G. Park, S.D. Tilley, H.J. Fan, M. Grätzel, *Science* 345 (2014) 1593–1596.
- [6] H. Zhou, F. Yu, J. Sun, H. Zhu, I.K. Mishra, S. Chen, Z. Ren, *Nano Lett.* 16 (2016) 7604–7609.
- [7] J. Li, H. Li, G. Zhan, L. Zhang, *Acc. Chem. Res.* 50 (2016) 112–121.
- [8] J. Suntivich, K.J. May, H.A. Gasteiger, J.B. Goodenough, Y. Shao-Horn, *Science* 334 (2011) 1383–1385.
- [9] D. Voiry, H. Yamaguchi, J. Li, R. Silva, D.C. Alves, T. Fujita, M. Chen, T. Asefa, V.B. Shenoy, G. Eda, *Nat. Mater.* 12 (2013) 850–855.
- [10] Z. Pei, H. Li, Y. Huang, Q. Xue, Y. Huang, M. Zhu, Z. Wang, C. Zhi, *Energy Environ. Sci.* 10 (2017) 742–749.
- [11] F. Yu, H. Zhou, Z. Zhu, J. Sun, R. He, J. Bao, S. Chen, Z. Ren, *ACS Catal.* 7 (2017) 2052–2057.
- [12] Y. Jia, L. Zhang, G. Gao, H. Chen, B. Wang, J. Zhou, M.T. Soo, M. Hong, X. Yan, G. Qian, *Adv. Mater.* 29 (2017) 1700017–1700024.
- [13] C. Tang, L. Gan, R. Zhang, W. Lu, X. Jiang, A.M. Asiri, X. Sun, J. Wang, L. Chen,

- Nano Lett. 16 (2016) 6617–6621.
- [14] J. Yin, Q. Fan, Y. Li, F. Cheng, P. Zhou, P. Xi, S. Sun, J. Am. Chem. Soc. 138 (2016) 14546–14549.
- [15] Y. Hou, M.R. Lohe, J. Zhang, S. Liu, X. Zhuang, X. Feng, Energy Environ. Sci. 9 (2016) 478–483.
- [16] C. Tang, R. Zhang, W. Lu, L. He, X. Jiang, A.M. Asiri, X. Sun, Adv. Mater. 29 (2017) 1602441–1602446.
- [17] S. Anantharaj, S.R. Ede, K. Sakthikumar, K. Karthick, S. Mishra, S. Kundu, ACS Catal. 6 (2016) 8069–8097.
- [18] X. Zou, X. Huang, A. Goswami, R. Silva, B.R. Sathe, E. Mikmeková, T. Asefa, Angew. Chem. 126 (2014) 4461–4465.
- [19] J. Wang, H.X. Zhong, Z.L. Wang, F.L. Meng, X.B. Zhang, ACS Nano 10 (2016) 2342–2348.
- [20] Y. Sun, S. Gao, Y. Xie, Chem. Soc. Rev. 43 (2014) 530–546.
- [21] Y. Zhao, X. Jia, G.I. Waterhouse, L.Z. Wu, C.H. Tung, D. O'Hare, T. Zhang, Adv. Energy Mater. 6 (2016) 1501974–1501993.
- [22] M.Q. Zhao, Q. Zhang, J.Q. Huang, G.L. Tian, J.Q. Nie, H.J. Peng, F. Wei, Nat. Commun. 5 (2014) 4410–4417.
- [23] M. Shao, F. Ning, J. Zhao, M. Wei, D.G. Evans, X. Duan, J. Am. Chem. Soc. 134 (2012) 1071–1077.
- [24] Z. Li, M. Shao, H. An, Z. Wang, S. Xu, M. Wei, D.G. Evans, X. Duan, Chem. Sci. 6 (2015) 6624–6631.
- [25] J. Jiang, A. Zhang, L. Li, L. Ai, J. Power Sources 278 (2015) 445–451.
- [26] F. Song, X. Hu, Nat. Commun. 5 (2014) 5477–5485.
- [27] Z. Wang, S. Zeng, W. Liu, X.W. Wang, Q. Li, Z. Zhao, F. Geng, ACS Appl. Mater. Interfaces 9 (2017) 1488–1495.
- [28] L. Yu, G. Li, X. Zhang, X. Ba, G. Shi, Y. Li, P.K. Wong, J.C. Yu, Y. Yu, ACS Catal. 6 (2016) 6444–6454.
- [29] N. Almana, S.P. Phivilay, P. Laveille, M.N. Hedhili, P. Fornasiero, K. Takanebe, J.M. Basset, J. Catal. 340 (2016) 368–375.
- [30] Y. Qu, H. Medina, S.W. Wang, Y.C. Wang, C.W. Chen, T.Y. Su, A. Manikandan, K. Wang, Y.C. Shih, J.W. Chang, Adv. Mater. 28 (2016) 9831–9838.
- [31] G. Shi, L. Yu, X. Ba, X. Zhang, J. Zhou, Y. Yu, Dalton Trans. 46 (2017) (2017) 10569–10577.
- [32] Z. Li, M. Shao, L. Zhou, R. Zhang, C. Zhang, J. Han, M. Wei, D.G. Evans, X. Duan, Nano Energy 20 (2016) 294–304.
- [33] X. Zhao, H. Zhang, Y. Yan, J. Cao, X. Li, S. Zhou, Z. Peng, J. Zeng, Angew. Chem. Int. Ed. 56 (2017) 328–332.
- [34] D. Kong, H. Wang, Z. Lu, Y. Cui, J. Am. Chem. Soc. 136 (2014) 4897–4900.
- [35] S. Li, Y. Wang, S. Peng, L. Zhang, A.M. Al-Enizi, H. Zhang, X. Sun, G. Zheng, Adv. Energy Mater. 6 (2016) 1501661–1501667.
- [36] X. Han, C. Yu, J. Yang, C. Zhao, H. Huang, Z. Liu, P.M. Ajayan, J. Qiu, Adv. Mater. Interfaces 3 (2016) 1500782–1500790.
- [37] S. Gao, Y. Lin, X. Jiao, Y. Sun, Q. Luo, W. Zhang, D. Li, J. Yang, Y. Xie, Nature 529 (2016) 68–71.
- [38] Z. Chen, D. Cummins, B.N. Reinecke, E. Clark, M.K. Sunkara, T.F. Jaramillo, Nano Lett. 11 (2011) 4168–4175.
- [39] H. Zhou, Y. Wang, R. He, F. Yu, J. Sun, F. Wang, Y. Lan, Z. Ren, S. Chen, Nano Energy 20 (2016) 29–36.
- [40] Z. Zhao, H. Wu, H. He, X. Xu, Y. Jin, Adv. Funct. Mater. 24 (2014) 4698–4705.
- [41] Z. Lu, W. Zhu, X. Yu, H. Zhang, Y. Li, X. Sun, X. Wang, H. Wang, J. Wang, J. Luo, Adv. Mater. 26 (2014) 2683–2687.
- [42] M.S. Faber, R. Dziejdz, M.A. Lukowski, N.S. Kaiser, Q. Ding, S. Jin, J. Am. Chem. Soc. 136 (2014) 10053–10061.



**Luo Yu** received his B.S. degree of Physics and Chemistry from Central China Normal University in 2013. He is now a Ph.D. candidate in both Prof. Ying Yu's group at Central China Normal University and Prof. Ren's group at University of Houston. His research focuses on the efficient non-noble metal catalysts for water splitting and CO<sub>2</sub> reduction in electrocatalysis and photocatalysis.



**Dr. Haiqing Zhou** is currently a postdoctoral fellow in Department of Physics and TcSUH at University of Houston. He received his Ph.D. degree in Prof. Lianfeng Sun's group in National Center for Nanoscience and Technology, Chinese Academy of Sciences in China in 2012, and a B.S. degree from Hunan Normal University, China in 2007. He joined Prof. Ren's group since 2014. His research mainly focuses on the synthesis of two-dimensional single crystals of layered transition-metal dichalcogenides, graphene, or other non-layered metal chalcogenides nanostructures, and embedding them into three-dimensional porous architectures for cathodic hydrogen evolution reaction or full water splitting.



**Jingying Sun** is currently a fifth year graduate student in Department of Physics and TcSUH at the University of Houston. She earned her B.S. degree in Physics at Jilin University, China. Her current research is mainly on materials for electrochemical applications and in-situ Transmission Electron Microscopy.



**Fan Qin** is currently a Ph.D. student under the supervision of Prof. Jiming Bao in Materials Science & Engineering at the University of Houston. He obtained his B.S. and M.S. degree from Wuhan Institute of Technology. His present research interests focus on the rational design of earth-abundant, high-efficient electrocatalysts and photocatalysts toward water splitting.



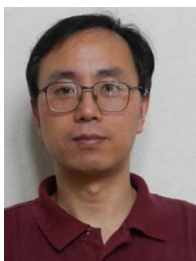
**Dan Luo** is currently a Ph.D. candidate of Chemical Engineering at University of Houston. He received his B.S. degree in Petroleum Engineering from Southwest Petroleum University, China. His research interest includes chemical functionalization of two dimensional materials and their applications, colloid and interface science, Janus particles, surface modification, enhanced oil recovery, etc. He is the recipients of CORA HAWLEY scholarship and PAUL C W CHU scholarship from Texas center of Superconductivity at University of Houston.



**Lixin Xie** received her B.S. degree in Polymetric Material and Engineering from Sun Yat-Sen University, China (2011) and M.S. degree in Material Science from University of Science and Technology of China, China (2014). She is currently a Ph.D. student in Dr. Shuo Chen's group. Her main research focuses on transmission electron microscopy and novel battery materials for energy storage.



**Dr. Fang Yu** is currently a postdoctoral fellow in Department of Physics and TcSUH at University of Houston, USA. She received his Ph.D. degree from National Center for Nanoscience and Technology, Chinese Academy of Sciences in China in 2012, a B.S. degree from Hunan Normal University, China in 2007. She joined Prof. Zhifeng Ren's group since 2013. Her research mainly focuses on the synthesis of vertically aligned carbon nanotube forests or individual single-walled carbon nanotubes and the unzipping of individual single-walled carbon nanotubes into graphene nanoribbons catalyzed by metal nanoparticles.



**Dr. Jiming Bao** is an associate professor of Electrical and Computer engineering at the University of Houston. He graduated from Zhejiang University with B.S. and M.S. in physics in 1992 and 1995, respectively. He obtained his Ph.D. in applied physics in 2003 from the University of Michigan, he then did post-doctoral research at Harvard University before joining the University of Houston in 2008 as an assistant professor. His current research covers many interdisciplinary topics ranging from solar energy conversion to fiber optic sensing. More information can be found from Dr. Bao's group website at <http://nano.ee.uh.edu/>.



**Dr. Shuo Chen** is currently an assistant professor in Department of Physics at the University of Houston. She obtained her B. S. in Physics from Peking University in China in 2002 and then Ph.D. in Physics from Boston College in 2006. From 2006–2011, she was a postdoctoral associate in the Department of Mechanical Engineering at MIT. Her research focuses on materials physics, especially synthesis and in situ electron microscopy of nanostructural materials for energy conversion and storage, such as thermoelectric materials, electrocatalysts, and batteries.



**Dr. Yong Li** is currently a professor of Atomic and Molecular Physics at Central China Normal University, China. He received his Ph.D. degree in Atomic and Molecular Physics from Wuhan Institute of Physics and Mathematics, Chinese Academy of Sciences in 1997. His research mainly includes theoretical study of quantum information and quantum calculation.



**Dr. Zhifeng Ren** is currently an M.D. Anderson Chair Professor in the Department of Physics and TcSUH at the University of Houston. He obtained his Ph.D. degree from the Institute of Physics Chinese Academy of Sciences, China in 1990. He was a postdoc and research faculty at SUNY Buffalo (1990–1999) before joining the Boston College as an Associate Professor in 1999. He specializes in thermoelectric materials, photovoltaic materials & systems, carbon nanotubes & semi-conducting nanostructures, efficient non-noble metal catalysts for water splitting, flexible transparent conductors, etc. More information can be found from Dr. Bao's group website at [https://mysm.uh.edu/wiki/projects/drrengroup/Dr\\_Rens\\_Group.html](https://mysm.uh.edu/wiki/projects/drrengroup/Dr_Rens_Group.html).



**Dr. Ying Yu** is currently a professor in College of Physical Science and Technology at Central China Normal University, China. He received her Ph.D. degree in Environmental Science from Nankai University in 1997. Her research mainly focuses on unique design of efficient nanomaterials for CO<sub>2</sub> reduction, water splitting and pollutants degradation; Nanostructural materials for energy storage; DFT calculations based on photocatalysis and electrocatalysis.